A joint time-scale representation methodology for the detection of acoustic gravity wave induced by solar eclipses

Stéphane Roux, Petra Sauli, Josef Boska, Patrice Abry

A joint time-scale representation methodology for the detection of acoustic gravity wave induced by solar eclipses

Stéphane G. Roux[1], Petra Šauli[2], Josef Boška[2], Patrice Abry[1]

[1] Laboratoire de Physique, CNRS UMR 5672
École Normale Supérieure de Lyon 46, allée d'Italie 69364 Lyon, France

[2]Institute of Atmospheric Physics ASCR, Czech Republic.

stephane.roux@ens-lyon.fr, Patrice.Abry@ens-lyon.fr
pkn@ufa.cas.cz, boska@ufa.cas.cz
Work supported by Grant CNRS/ASCR 18098 and GACR project 205/06/1618

Résumé − Nous proposons l'utilisation de la transformée en ondelettes complexes pour détecter et caractériser la propagation d'ondes gravito-acoustiques dans l'ionosphère, à partir de données représentant les fluctuations temporelles de concentrations électroniques à différentes altitudes. Nous détectons d'abord, à chaque altitude, les maxima locaux des transformées. Les maxima qui existent simultanément à différentes altitudes dans un même voisinage temps-fréquence sont ensuite rassemblés dans une même structure. La dérivation de la phase des coefficients en ondelettes le long de ces lignes de maxima nous permet d'extraire les paramètres de propagation. Cet outil est utilisé pour étudier trois éclipses solaires différentes. Cela nous permet de mettre en évidence l'occurrence d'ondes gravito-acoustiques durant ces événements.

Abstract − We introduce a wavelet-based methodology to detect and characterize acoustic-gravity waves propagating through Ionosphere. It is based on data consisting of the time fluctuations of electron concentrations at different heights, collected from vertical Ionospheric sounding. First, we detect the local maxima of the continuous complex wavelet transforms, separately at each heights. Second, we connect the maxima that exist jointly within the same time-period neighborhood, over a continuous range of heights. From the derivation of the phases of the wavelet transform along these maxima lines, we extract the propagation parameters. This methodology is applied to the data collected during three different solar eclipses. It enables us to evidence the existence of several acoustic-gravity waves during these events.

1 Motivation

The interest for short time variabilities in Ionospheric attributes is related to the role that Ionosphere plays on the Earth's environment and space weather. Acoustic-gravity waves (AGW) are the sources of most of the short-time Ionospheric variability and play an important role in the dynamics and energetics of Atmosphere and Ionosphere. Many different mechanisms are likely to contribute to AGW generation: for instance, excitation at high latitudes induced by geomagnetic and consequent auroral activity, meteorological phenomena, excitation in situ by solar terminators and by the occurrence of solar eclipses [1]. For this latter example, the lunar shadow creates a cool spot that sweeps at supersonic speed across the Earth. The sharp border between sunlit and eclipsed regions, defined by strong gradients in temperature and ionization flux, moves throughout Atmosphere and drives it into a non-equilibrium state. AGW contributes to the return to equilibrium [2]. Although mechanisms are not well understood, several studies [3, 4, 5] showed direct evidence that solar eclipses induce AGW. The present article consist of a methodological contribution to the analysis of the relations between solar eclipses and AGW.

Previous technics proposed to detect and characterize AGW were mostly based on Fourier transforms of the data [4, 6, 7]. However, by definition, Fourier transforms are averaging, and hence mixing information, along time. When two waves exist at different time positions with close characteristic frequencies, the wave propagation parameters measured at a given frequency are likely to be biased by the superimposition. To overcome such drawbacks, we recently proposed to use wavelet, instead of Fourier, decompositions [8, 9]. This enables us to disentangle the contribution of different structures and to perform more accurate detections and analysis of wave structures. A MATLAB toolbox developed by ourselves provides us an efficient wave analysis tool with the visualization of the data and of the structure therein. The present contribution is a continuation of [8, 9], with focus on data analysis and detection issues.

2 Acoustic-Gravity Wave theory

The propagation of AGW is dispersive and non linear. It is characterized by the following dispersion relation:

$$\omega^4 - \omega^2\omega_a^2 - k_x^2C^2(\omega^2 - \omega_g^2) - C^2\omega^2k_z^2 = 0, \qquad (1)$$

where k_x and k_z stand for the horizontal and vertical components of the wave vector, C for the speed of sound, ω_a for the angular acoustic cut-off frequency and ω_g for the angular buoyancy (or Brunt-Väisälä) frequency. It accounts for the existence of two propagation frequency ranges: acoustic modes, with characteristic frequencies

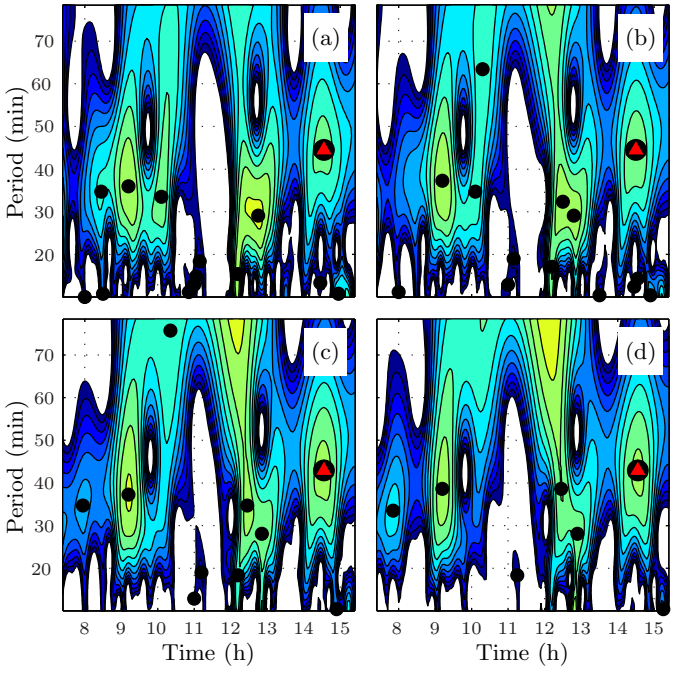

FIG. 1: **Scalograms:** Examples of scalogram plots at four consecutive heights 200 km (a), 205 km (b), 210 km (c) and 215 km (d); Local maxima line are marked with "●". Around 14h30 min UT, there exists a well developed line of local maxima, marked with a "●", that coincide in time and period over a significant range of heights z.

larger than the acoustic cut-off ω_a, gravity modes, with characteristic frequencies smaller than the Brunt-Väisälä ω_g. For further details on AGW theory, the reader is referred to e.g., [10, 11].

3 Measurements and time series

Three different solar eclipses are analyzed: two of them are total solar eclipses (11 August 1999 and 29 March 2006) and one is annular (3 October 2005). Measurements are performed at the European mid-latitude Ionospheric station Průhonice (Czech Republic; 49.9N, 14.6E), using vertical Ionospheric sounding techniques. From the vertical profiles of electron concentrations, real height vertical electron density profiles are derived, as a function of time t, at fixed heights z: $X(t,z),\ t \in [T_m, T_M], z \in \mathbb{Z}$. T_m and T_M denote the beginning and end of the measurement in UT. The spatial sampling period is 5km, corresponding to heights $\mathbb{Z} = \{155, 160, 165, \ldots, 255\}$ (in km). The time sampling period is one minute for the 1999 eclipse and two minutes for the two others.

4 Detection and characterization

4.1 Representing

To analyze the data $X(z,t)$, one classically uses a wave packet expansion by means of Fourier Transforms:

$$X(z,t) = \int_{\omega_0(z)-\Delta\omega}^{\omega_0(z)+\Delta\omega} X_0(\omega, z) \exp \imath(\omega t - kz)\ d\omega, \quad (2)$$

where $X_0(\omega, z)$ denotes the amplitude of the wave, obtained as the Fourier transform of $X(z,t)$ with respect to the time variable t, $\omega_0(z)$ and $\Delta\omega$ stand respectively for the central frequency and characteristic frequency width of the wave packet at altitude z. Instead, we proposed, in [8, 9], to extend this original idea to the wavelet framework. This enables us to obtain a joint time and frequency description of the data and hence to better detect and characterize waves whose existence is transient in time and whose energy is mostly concentrated in a given frequency band. The coefficients of the continuous complex wavelet transform are obtained by comparison of the data $X(t,z)$, by means of inner product, against dilated and translated version of a generating function $\psi_0(t)$ called mother wavelet :

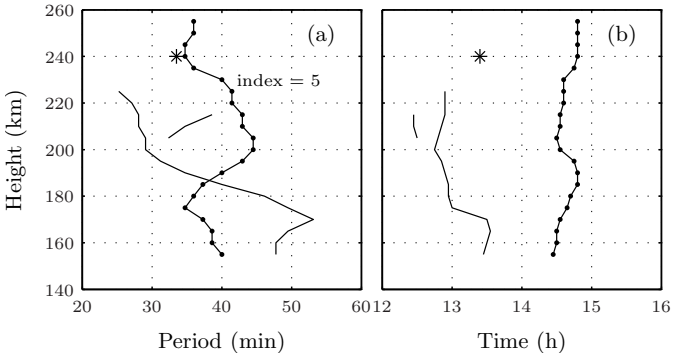

FIG. 2: **Maxima lines:** Visualization of the maxima lines detected for 12h $\leq t \leq$ 16h and 20min $\leq P \leq$ 60min. One can decide to select a particular wave via a simple *click* on the corresponding line in either plot.

$$T_X(a,t,z) = \int_{\mathbb{R}} X(u,z) \frac{1}{\sqrt{a}} \psi_0 \left(\frac{u-t}{a} \right) du. \quad (3)$$

One can relabel, with a little abuse of notation, the wavelet coefficients $T_X(a,t,z) \equiv T_X(\omega,t,z)$ using the usual scale-frequency conversion: $\omega = \omega_\psi / a$, where ω_ψ is the central pulsation of the chosen mother-wavelet (that one can easily compute either analytically or numerically). Let $\{|T_X(\omega,t,z)|, \phi(\omega,t,z)\}$ denote the modulus and phase of the complex wavelet coefficients. Scalograms (as shown in Figs. 1 and 3), consist of the plots of $|T_X(\omega,t,z))|$ as a function of time t and period $P = 2\pi/\omega = 2\pi a/\omega_\psi$. Therefore, the scalograms $|T_X(\omega,t,z))|$ can be given the meaning of energy content of X, at height z, around time position t and around frequency $\omega = \omega_\psi / a$.
We used both Paul and Morlet mother-wavelets. For simplicity, all plots shown here are based on Paul wavelet ($N = 6$), defined as $\psi_{0,N}(t) = \frac{2^N \imath^N N!}{\sqrt{\pi(2N)!}}(1-\imath t)^{-(N+1)}$, where the parameter N mostly controls its time supports, that can hence be easily tuned to a given purpose.

4.2 Detecting

For each altitude z independently, a high-pass filter is applied to the time series $X(t,z)$ to suppress periods larger than 90 min. Then, complex continuous wavelet coefficients $T_X(a,t,z)$ are computed on these detrended data. For each scalogram $|T_X(a,t,z))|$ separately, local energy maxima are detected and recorded. Beginning at the lowest height z, we seek, for each detected maximum, the nearest maximum existing at the next upper height (top to bottom chaining). When several maxima from a given

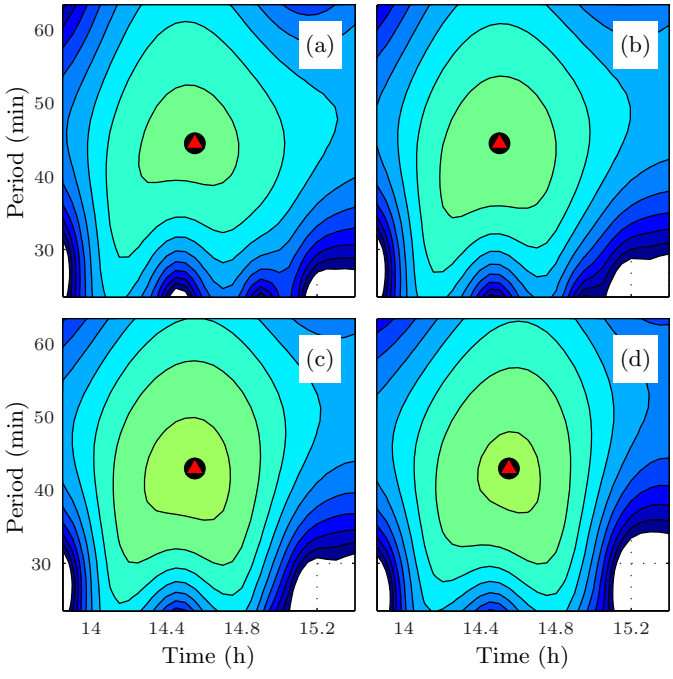

FIG. 3: Same scalograms as these in Fig. 1 but zoomed around the structure marked with a "●" in Fig. 1 and characterized in Figs. 4 and 5.

height are connected to the same maximum at the next height, only the one closer to this latter is retained (bottom to top final chaining). Then, we proceed successively to the next heights z to obtain a set of maxima lines. Each maxima line corresponds to the detection of a wave, whose structure is enclosed in a collection of attributes: time and period positions, and amplitudes of the maxima, as functions of z, for the range of altitudes within which the maxima line exists: $z \in [\underline{z}, \overline{z}]$. This local maxima detection and chaining operations are sketched in Figs. 1, 2 and 3. Fig. 1 shows scalograms obtained at (4 out of 21) different heights for the whole observation duration. Black dots correspond to the different detected waves. Our MATLAB toolbox enables the visualization of the set of the maxima line detected in a given time and period neighborhood, with respect to different attributes. For instance, Fig. 2 shows the maxima lines detected after noon ($12\text{h} \leq t \leq 16\text{h}$) and for periods between 20 and 60 minutes. Two interesting structures (persisting over several consecutive heights) are visible. The star corresponds to an isolated maximum at $z = 240$ km. The selection of a particular wave, one wishes to analyze, can be achieved by a simple *click* on the corresponding line. In turns, this produces automatically scalogram plots in Fig. 3, consisting of zoomed versions of those in Fig. 1. This enables to validate the choice of the waves one intends to analyze.

4.3 Characterizing

When clicking on a chosen maxima line in Fig. 2, we also obtain a measure of the direct attributes of the waves, shown in Fig. 4. First, from the information collected for each wave, we derive the mean time t_0 and the mean pulsation ω_0 where the mean is taken over the range of altitude $z \in [\underline{z}, \overline{z}]$ (cf. Fig. 4 top row). Second, within a chosen time-pulsation neighborhood centered on (t_0, ω_0), we compute separately for each triplet (ω, t, z) the z-components of the:

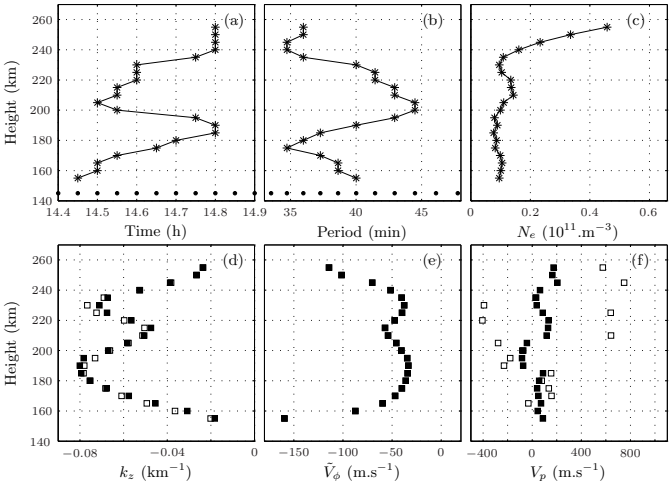

FIG. 4: Wave parameters measured : Time location (a), period (b) and amplitude (c) of the detected wave. Bottom row, median (black symbols) and averaged (white symbols) value of the vertical components of the wave vector (d), phase velocity (e) and packet velocity (f).

- wave vector : $k_z(\omega, t, z) = \partial\phi(\omega, t, z)/\partial z$,
- phase velocity : $v_\phi^{(z)}(\omega, t, z) = \omega / k_z(\omega, t, z)$,
- packet velocity : $v_{p,z}(\omega, t, z) = \partial\omega / \partial k_z(\omega, t, z)$.

Then, we compute the averaged and median values of these quantities over this chosen narrow time-pulsation neighborhood, i.e., over t and ω, for each z. Comparing the median and averaged values enable us to assess the correctness of the choice of the neighborhood, median value being less dependent on outliers. For example, Fig. 4 (bottom row) shows that the median (black symbols) and averaged (white symbols) values, computed with the time-scale neighborhood shown in Fig. 3, are very similar except for packet velocity. The median value provides us with more robust results. Note that to compute the propagation parameters, we use only the phase of the wavelet transforms. To obtain phase velocity, we need one derivation, while packet velocity involves a double derivation. Derivation is performed using a third-order or fifth-order finite difference procedure, depending on the range of heights available. The double derivation is numerically poorly conditioned if the sampling period of the data is close to the period of the studied structure. In that case, this procedure may lead to inaccurate results. This is corrected with the use of the modeling described in the next section.

4.4 Modeling

To decide whether a detected wave corresponds or not to the propagation of an acoustic-gravity wave, it can be compared to the theoretical acoustic-gravity wave propagation model [9]. By injecting $k_z(\omega, t, z)$ in Eq. (1), we obtain, for each triplet (ω, t, z), the $x-$component of the wave vector. Making use of a set of classical AGW propagation equations not recalled here (cf. e.g., [9, 10, 11]), we obtain the phase and packet velocity $z-$ and $x-$

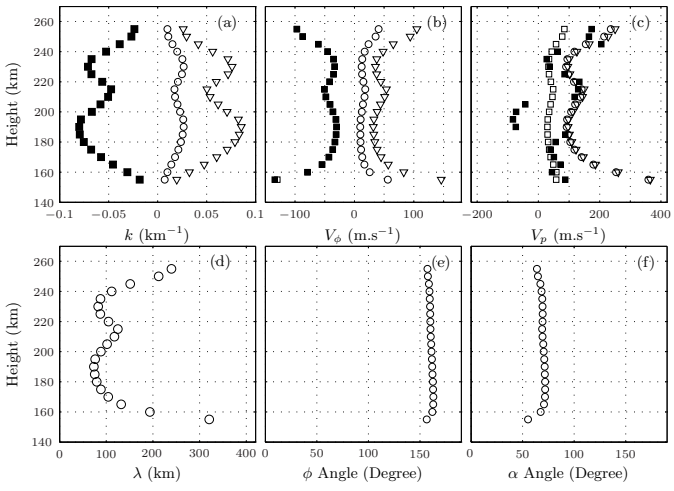

FIG. 5: Wave parameters computed from the AGW theory: Wave vector (a), Phase velocity (b), packet velocity (c), wave number (d), energy (e) and phase (f) angles. For the vectors of first row, the '□' correspond to the measured (black) and computed (white) $z-$components, the '○' correspond to the horizontal components while the '▽' are related to the modulus.

components as well as the phase and energy propagation angles, Φ and α, respectively, measured from the vertical, clock-wise. An important property of gravity waves consists of the fact that the phase propagates downward while the wave is moving upward or vice versa; while for acoustic wave, phase and packet velocities travel in the same direction. As in the previous stage, the crucial point is that we compute each of these quantities separately for each triplet (ω, t, z) and then take the median value on the chosen time-scale neighborhood. Fig. 5 shows, for the chosen wave, the propagation parameters obtained with this procedure and using the same time-scale neighborhood as that in Fig. 4. Results are shown here for the 2006 solar eclipse only and for a single wave, for space reasons. Equivalent plots are obtained for different waves detected on each eclipse (cf. [9]). Equivalent plots for each of the detected structures can be found at *http://www.ufa.cas.cz/html/climaero/sauli.html*.

5 Results and Conclusions

In the present contribution, we showed that, taking advantage of the excellent joint time and frequency localization properties of the wavelet transform, we are able to detect and characterize wave structures. A key point in our approach lies in the use of sequences of vertical profiles of electron concentration and the application of a median filter over a narrow neighborhood. Our methodology enables us to detect several gravity waves generated during and after solar eclipses and one acoustic wave. Acoustic waves have short periods (of the order of a few minutes), so that it is only the joint use of a 1-min sampling period together with a joint time and period representation tool that enabled the detection. As far as we know, this had not been achieved before. The MATLAB toolbox is available upon request.

References

[1] G. Chimonas, C.O. Hines. *Atmospheric Gravity Waves Induced by a Solar Eclipse.* Journal of Geophysical Research, 75, 4, 875-875, 1970.

[2] S. Kato, T. Kawakami, D. St. John. *Theory of gravity wave emission from moving sources in the upper atmosphere.* Journal of Atmospheric and Terrestrial Physics, 39, 581-588, 1977.

[3] G.O. Walker, T.Y.Y. Li, Y.W. Wong, T. Kikuchi, Y.N. Huang. *Ionospheric and Geomagnetic Effects of the Solar Eclipse of 18 March 1988 in East-Asia.* Journal of Atmospheric and Solar-Terrestrial Physics, 53 (1-2), 25-37, 1991.

[4] J.Y. Liu, C.C. Hsiao, L.C. Tsai, C.H. Liu, F.S. Kuo, H.Y. Lue, C.M. Huang. *Vertical Phase and Group velocities of internal gravity waves derived from Ionograms during the solar eclipe of 24 october 1995.* Journal of Atmospheric and Solar-Terrestrial Physics, 60, 1679-1686, 1998.

[5] T. Farges, J.C. Jodogne, R. Bamford, Y. Le Roux, F. Gauthier, P.M. Vila, D. Altadill, J.G. Sole, G. Miro. *Disturbances of the western European Ionosphere during the total solar eclipse of 11 August 1999 measured by a wide Ionosonde and radar network.* Journal of Atmospheric and Solar-Terrestrial Physics, 63 (9), 915-924, 2001.

[6] D. Altadill, J.G. Sole, E.M. Apostolov. *Vertical structure of a gravity wave like oscillation in the Ionosphere generated by the solar eclipse of August 11, 1999.* Journal of Geophysical Research - Space Physics, 106 (A10), 21419-21428, 2001.

[7] D. Altadill, F. Gauthier, P. Vila, J.G. Sole, G. Miro, R. Berranger. *The 11.8.1999 solar eclipse and the Ionosphere: a search for distant bow-wave.* Journal of Atmospheric and Solar-Terrestrial Physics, 63 (9), 925-930, 2001.

[8] P. Šauli, P. Abry, J. Boška, L. Duchayne. *Wavelet Characterisation of Ionospheric Acoustic and Gravity Waves occuring during the Solar Eclipse of August 11, 1999.* Journal of Atmospheric and Solar-Terrestrial Physics, 68, 586-598, 2006.

[9] P. Šauli, S.G. Roux, P. Abry, J. Boška, *Acoustic-gravity waves during solar eclipses: detection and characterization using wavelet transforms.* Journal of Atmospheric and Solar-Terrestrial Physics, preprint.

[10] K. Davies. *Ionospheric Radio.* Peter Peregrinus Ltd, London, UK, 1990.

[11] C.O. Hines. *Internal atmospheric gravity waves at Ionospheric heights.* Canadian Journal of Physics, 38, 1441-1481, 1960.

[12] J.E. Titheridge. *Ionogram analysis with the generalised program POLAN.* UAG report-93, 1985.

[13] X. Huang, B.W. Reinish. *Vertical electron density profiles from the digisonde network.* Advances in Space Research, 18(6), 121-129, 1996.